Journal of Nanoparticle Research (2006) 8: 323–333
DOI 10.1007/s11051-005-9007-z

Visibly transparent & radiopaque inorganic organic composites from flame-made mixed-oxide fillers

Lutz Mädler[1,4,*], Frank Krumeich[2], Peter Burtscher[3] and Norbert Moszner[3]
[1]*Department of Mechanical and Process Engineering, Particle Technology Laboratory, ETH Zürich, CH-8092, Switzerland;* [2]*Department of Chemistry and Applied Biosciences, Laboratory of Inorganic Chemistry, ETH Zürich, CH-8093, Switzerland;* [3]*Ivoclar Vivadent AG, Schaan, FL-9494, Liechtenstein;* [4]*Department of Chemical Engineering, University of California, Los Angeles, 5531-G Boelter Hall, Los Angeles, CA 90095, USA; Author for correspondence (Tel.: +41-310-825-9926; Fax: +41-310-206-4107; E-mail: lutz@seas.ucla.edu)*

Received 15 October 2004; accepted in revised form 6 July 2005

Key words: composite, dental materials, flame spray pyrolysis, radiopaque

Abstract

Radiopaque composites have been produced from flame-made ytterbium/silica mixed oxide within a crosslinked methacrylate resin matrix. The refractive index of the filler powder increased with ytterbium oxide loading. A high transparency was achieved for a matching refractive index of the filler powder and the polymer in comparison to commercial materials with 52 wt% ceramic filling. It was demonstrated that powder homogeneity with regard to particle morphology and distribution of the individual metal atoms is essential to obtain a highly transparent composite. In contrast, segregation of crystalline single-oxide phases drastically decreased the composite transparency despite similar specific surface areas, refractive indices and overall composition. The superior physical strength, transparency and radiopacity compared to composites made from conventional silica based-fillers makes the flame-made mixed-oxide fillers especially attractive for dental restoration materials.

Introduction

Tailor made inorganic/organic composites have received increasing attention in recent years because of their wide range of applications such as for optics (Choudhury et al., 2003), sensors and catalysts (Boury & Corriu, 2000), mechanics and biomedicine (Asefa et al., 2000; Moszner & Klapdohr, 2004). Transparency towards visible light is a key issue in many composite applications (Nussbaumer et al., 2002). A specific example is the application of composite materials in dental restorations where transparent composites can be modified to any tooth shade for excellent esthetical properties. Moreover, functional composites require high strength, high hardness and low wear, which is readily achieved for filler particles in the nanometer range (Combe et al., 1999; Zantner et al., 2004). An additional requirement in dental (and other biomedical) applications is the radiopacity of such composite materials (Moszner & Salz, 2001; Klapdohr & Moszner, 2005). Radiopacity is enhanced by incorporation of atoms with a high proton number which effectively absorb the

X-rays. Currently, silica fillers are widely used in composite manufacture because of their well studied silanization mechanisms resulting in excellent polymer/filler physical properties and their availability in the nanometer size range. However, silica has a much lower refractive index (1.46) than commonly used monomers such as a mixture of Bis-GMA and triethylenglycol dimethacrylate (1.53). This mismatch leads to a reduced transparency because of light interaction at the polymer/filler interface. Another disadvantage of pure silica fillers is inherent low radiopacity.

Therefore, mixtures of inorganic silica-based fillers are often utilized for dental applications. The addition of high proton number compounds accompanied with a high refractive index such as YbF_3 (Rheinberger et al., 1999) or Ta_2O_5 (Schulz et al., 2005) enables control of the mixture refractive index and provides sufficient radiopacity. It has been shown recently that flame-made fillers can be uniformly dispersed in a dimethacrylate resin polymer networks increasing the elastic modulus of the resulting composite (Mueller et al., 2004). Utilizing the versatile and scalable flame spray pyrolysis (FSP) technique enables the synthesis of non-porous mixed-oxide nanoparticles. Control of FSP parameters with respect to the resulting product properties has been investigated extensively in the past (Mädler et al., 2002a). It has further been shown that the refractive index of these materials can be controlled by the mixed-oxide composition (Morse, 2003; Schulz et al., 2005). Here FSP is used for production of an ytterbium oxide-mixed silica filler. The importance of process and quality control for such materials is investigated.

Furthermore, flame synthesis of ytterbium silica mixed-oxide can be utilized in other applications where the Yb/Si-mixed oxide is known to improve mechanical properties of silicon nitride (Klemm & Pezzotti, 1994; Liang et al., 1999; Guo et al., 2001), to catalyze α-pinene-isomerization reaction (Yamamoto et al., 1999a), and to improve optical data transfer (Wu et al., 1995; Hehlen et al., 1997).

Experimental

Precursor preparation

The mixed ytterbium-oxide/silica powders were prepared from two different precursor mixtures. Both mixtures had a constant total metal loading and a constant enthalpy of combustion for all Si/Yb mixing ratios which were varied in order to obtain ytterbium oxide (Yb_2O_3) mass loadings (X_{wt}) from 0 to 0.5 ($X_{wt} = m_Yb_2O_3/m_Yb_2O_3 + m_{Sio_2}$)). In all experiments, tetraethyl orthosilicate (TEOS, Aldrich, purity 98%) and ytterbium nitrate pentahydrate ($Yb(\{NO_3)_3 \cdot 5H_2O$, Rhodia, purity 99.9%) were used as primary Si and Yb sources, respectively.

In a first experimental series, appropriate amounts of $Yb(NO_3)_3 \cdot 5H_2O$ were dissolved in a mixture of 59.2 vol% acetonitrile (Fluka, purity 99.9%), 34.2 vol% acetic anhydride (Aldrich, purity 99%) and 6.6 vol% acetic acid (Fluka, purity 99.5%) to obtain a 0.5 M ytterbium solution with a combustion enthalpy of 19 kJ/ml. The mixture was heated to 60°C to enable complete dissolution of the ytterbium nitrate pentahydrate and complete dissolution was maintained after cooling to room temperature. TEOS (11.6 vol%) was mixed with 51.8 vol% acetonitrile and 36.6 vol% acetic anhydride to obtain a 0.5 M silicon solution with a combustion enthalpy of 19 kJ/ml. Both solutions were mixed according to the desired Yb/Si ratio. In this way the total energy content of the precursor solution (0.5 M) was kept constant (19 kJ/ml) for all Yb/Si ratios. This solution will be referred to as "Nitrile solution" throughout the following discussion.

In a second experimental series, a mixture of 0.25 M ytterbium nitrate pentahydrate in 18.75 vol% acetic anhydride and 81.25 vol% 2-ethylhexanoic acid (2-EHA, Riedel-de Haën, purity 99%) was prepared and heated in a silicon oil bath at 107°C under constant nitrogen flow. Exchange of the nitrate with the ethylhexanoate ligand proceeded via reactive distillation at the temperature of 107°C. Non-reacted crystal water, acetic acid, nitric acid and NO_x were distilled during the reactions enabling the formation of the Yb-ethylhexanoate. All water was removed from the ytterbium precursor during this distillation step. TEOS and xylene (Riedel-de Haën, purity 96%) were mixed (55:45 by volume) and added in appropriate amounts to the ytterbium solution. For precursor solutions with $X_{wt} < 0.5$, a mixture of acetic anhydride and 2-ethylhexanoic acid (3:13 by volume) were combined to obtain the final 0.5 M metal concentration. In this way the total combustion energy content of the precursor

solution (0.5 M) was kept constant (31 kJ/ml) for all Yb/Si ratios between 0 and 0.5. This solution will be referred as "2-EHA solution" throughout the following discussion.

Filler preparation and characterization

Powder synthesis was performed using a FSP reactor described elsewhere (Mädler et al., 2002a, b). A concentric supporting flamelet ring was formed from premixed methane/oxygen ($CH_4 = 1.5$ l/min, $O_2 = 3.2$ l/min). Water cooling of the reactor avoided any evaporation of the precursor within the precursor feed lines. The liquid precursor was fed by a syringe pump with a rate of 5 ml/min and was dispersed by 5 l/min (if not stated otherwise) of oxygen (Pan Gas, purity $>99.95\%$) into fine droplets by the gas-assist nozzle (pressure drop 1.5 bar). In order to assure sufficient oxidant for complete conversion of the reactants, an additional outer oxygen flow (5 l/min) was supplied. The product powder was collected on a glass fiber filter (GF/D Whatman, 257 mm in diameter) with the aid of a vacuum pump. During the experiment the filter was placed in a water cooled holder 400 mm above the nozzle, keeping the off-gas temperature below 200°C.

X-ray diffraction (XRD) patterns were recorded from $2\Theta = 20$ to 70° with a Bruker, AXS D8 Advance (40 kV, 40 mA, step size 0.03°, scan speed 0.60°/min, Cu Kα radiation). Transmission electron microscopy (TEM; Philips CM30, LaB 6 cathode, 300 kV) was used to image the particle morphology. Elemental concentrations at selected positions in the TEM images were determined by energy-dispersive X-ray spectroscopy (EDXS, Fa. Noran detector). Element-specific images were also obtained by means of the electron spectroscopic imaging (ESI) technique with an energy filter (Gatan imaging filter) installed on a Philips Tecnai F30 microscope (field emission cathode, 300 kV). The three-window method for the mapping and compensation for specimen drift was applied as described in detail elsewhere (Krumeich et al., 2000). Edge onsets were chosen at 1839 eV and 1528 eV for Si–K and Yb–$M_{IV,V}$, respectively. The morphology of product powder was further examined using scanning electron microscopy (SEM, Hitachi, S-900). The samples for SEM analysis were prepared by platinum sputtering (2 nm layer thickness).

The BET specific surface area (SSA), was measured by nitrogen adsorption at 77 K (Micromeritics Gemini 2375) after degassing the powder sample, for 1 h at 150°C in nitrogen. The average BET-equivalent particle diameter, d_{BET}, was calculated from the formula $d_{BET} = 6/(\mathrm{SSA}\ \rho_p)$, assuming spherical, monodisperse particles, where ρ_p is the density of the mixed-oxides according to their mass ratio ($\rho_{Yb2O3} = 9.2\,\mathrm{g/cm^3}$; $\rho_2 = 2.2\,\mathrm{g/cm^3}$).

Refractive index measurements of the filler materials was performed by applying the Becke-Line method, often called central illumination method (Stoiber & Morse, 1994). When a light microscope is focused on the grain of interest, a bright line (Becke line) is observed along the border of the grain. As the object is moved towards the condenser lens, a movement of the Becke line can be observed. If the grain material has higher (or lower) refractive index than the surrounding medium the Becke line moves inwards (or outwards). This method has been used successfully for determination of refractive indices of synthetic fibers (McLean, 1965) and aromatic polyimides (Simpson & St. Clair, 1997). However, for small particles, i.e. $<50\ \mu$m, the Becke-Line method appears to be problematic since particles could optically dissolve into the organic liquid and no sharp grain edge can be identified (Saveyn et al., 2002). To overcome this problem, a defined amount of the powder sample (17 mg, if not stated otherwise) was pressed into a thin tablet (13 mm in diameter) using a manually operated hydraulic press (Specac) with a pressure of 370 MPa (if not stated otherwise). In this way, sharp edges and smooth fracture planes were obtained. The measurements were performed with a petrographic microscope (Axioplan, Zeiss) using a 10× objective. Standardized refractive index liquids (Cargille Laboratories, Inc.) were used as immersion media and temperature was maintained at 21°C. Measurements were performed under monochromatic light using a NaD filter, 589 nm.

Composite preparation and characterization

The composite was prepared by treating the surface of the ceramic nanoparticle fillers with

γ-methacryloxypropyltrimethoxysilane (Union Carbide) to improve the bonding with the monomer matrix. After mixing bisphenol-A-diglycidyldimethacrylate (ESSCHEM), urethane dimethacrylate (Ivoclar Vivadent) and decandiol dimethacrylate (Ivoclar Vivadent) at a ratio of 4:3:2 (by weight), 0.3 wt% camphorquione (Rahn) and 0.6 wt% N,N-cyanoethylmethylanilin (Lonza) were dissolved in the monomer mixture. The composite was made by adding the Yb/Si-mixed oxide filler to the monomer mixture and stirring the mixture under vacuum in order to avoid air bubbles. For transparency screening of the composites a filler loading of 16.5 wt% was used while comparison with commercial filling materials, 52 wt% of the Yb/Si-mixed oxide was used. For 16.5 wt% filler loading the inorganic particles are not to be silanized in order to avoid an agglomeration affect of the small particles used. Composites with commercial fillers were prepared from SiO_2 filler (OX-50, Degussa) (52 wt%) and a mixed standard YbF_3/SiO_2 filler using OX-50 (35 wt%) and YbF_3 (Rhodia) (15 wt%). The composite was polymerized with a dental curing unit (Ivoclar Vivadent, Astralis 10, 1100 mW/cm^2) with a curing time of 20 s.

The composite transparency was measured in transparent mode with a Minolta CT-310 analyzer. A xenon lamp was used as light source which has a similar spectrum as sun light (Minolta). The transparency measurements were calibrated to 100% transparency with a water filled cuvette (1 mm thickness). The composite transparencies were obtained from 1 mm-thick samples after calibration. The thickening behavior of the monomer/filler paste was measured with the disc-consistency method. The paste (100 mg) was placed between two glass plates with a load of 120 g over a period of 3 min. The paste deformed into a circular disc while the disc diameter represents the thickening behavior. A thin disk (large diameter) indicates a low degree of paste thickening, giving improved paste processing. Flexural strength and elastic E-modulus were measured using Z010 universal testing machine (Zwick) after polymerization of 25×2×2 mm bars twice for 3 min and storage for 24 h in water at 37°C. The X-ray radiopacity was compared to an aluminum calibration standard consisting of known thicknesses where 0.5 mm corresponds to a radiopacity of 50%.

Results

Validation of refractive index method

The procedure of the refractive index measurements was validated for the ultrafine particles used in this study. Figure 1 shows the measured refractive index obtained with the Becke line method for two different samples as a function of the applied pressure during tablet preparation. Varying the pressure by three orders of magnitude has no detectable influence on the refractive index as shown for FSP-made pure SiO_2 (SSA = 281 m^2/g) and Yb/Si-mixed oxide ($X_{wt} = 0.1$, SSA = 380 m^2/g) powders. The tablet thickness also has no significant influence on the obtained refractive index as shown for three different tablet masses of 10, 17 and 30 mg of the Yb/Si-mixed oxide ($X_{wt} = 0.1$) powder. The absolute value of the refractive index measurement was crosschecked with literature data for six different compounds with a refractive index in the range from 1.445 to 1.767. Figure 2 shows a comparison of the refractive index measured using the Becke line method and the corresponding literature values for MgO, $Mg(OH)_2$, SiO_2, α-quartz (Wypych, 1999) and the ytterbium silicates (Toropov & Bondar, 1961). Magnesium oxide (MgO) and magnesium hydroxide ($Mg(OH)_2$) were purchased from Sigma-Aldrich (purity >95%) while

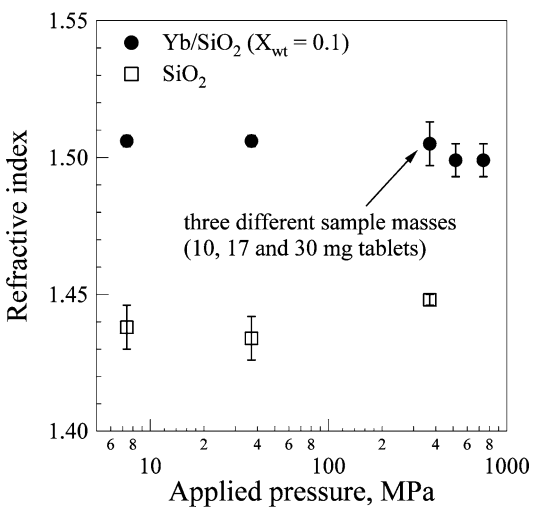

Figure 1. Effect of applied pressure during pellet preparation on the obtained refractive index measured by the Becke line method.

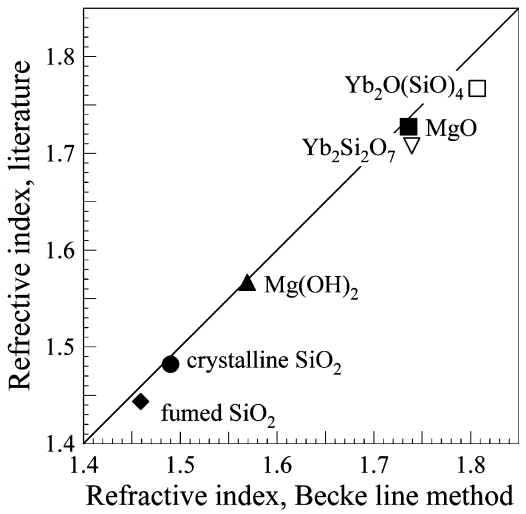

Figure 2. Comparison of powder refractive index measured by the Becke line method and reported literature values of the corresponding bulk material (closed symbols (Wypych, 1999); open symbols (Toropov and Bondar, 1961)).

fumed silica was used as prepared by the FSP method using the "Nitrile solution": crystalline SiO_2 (α-quartz) and the two ytterbium silicates ($Yb_2Si_2O_7$, $Yb_2O[SiO_4]$) were prepared by the FSP method according to their weight fractions ($X_{wt} = 0$, 0.766 and 0.868, respectively) from the "Nitrile solution" and calcined for 2 h at 1200°C (temperature ramp 5 K/min) to obtain the desired crystal structure (verified by XRD). The maximum deviation between the determined refractive index from the powder samples and the literature values was −0.04. The deviation decreases for smaller refractive indices, while in the range of interest for this study (1.53) the deviation was only −0.015 (1% of total value). Measured values were systematically lower than the corresponding literature values. This systematic deviation may be attributed to air captured in the pores between the fine particles, even after pressing, leading to an overall smaller refractive index since the Becke line method results in an average value.

Mixed-oxide filler properties

Powder synthesis from the "Nitrile solution" resulted in an inhomogeneous particle morphology. The powder consisted of a mixture of particles smaller than 10 nm and larger particles in the size range from 50 to 200 nm. Figure 3 shows a corresponding TEM image of such a powder. The EDXS analysis within area A reveals that the small particles consist of ytterbium oxide and silica whereas all larger particles consist of ytterbium oxide only (EDX of area B). In contrast, homogeneous powders were obtained from the "2-EHA solution". A direct comparison of the Yb/Si-mixed oxide ($X_{wt} = 0.5$) powder morphology synthesized with either the "Nitrile solution" or the "2-EHA solution" is shown in Figures 4a and b, respectively. The powder derived from the "2-EHA solution" (Figure 4b) does not show any

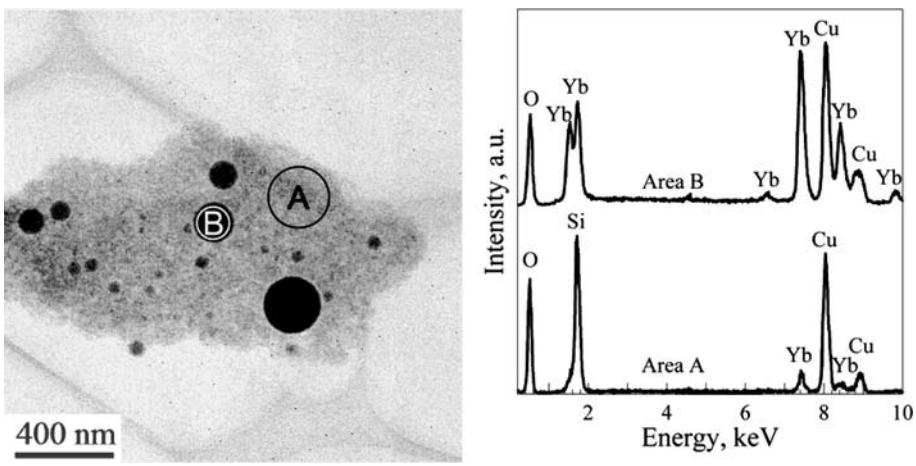

Figure 3. TEM image and corresponding EDX spectra taking in area A and B (as indicated in TEM) of FSP Yb/Si-mixed oxide ($X_{wt} = 0.2$) powder prepared with the "Nitrile solution". The observed Cu-signals resulted from the TEM copper grid.

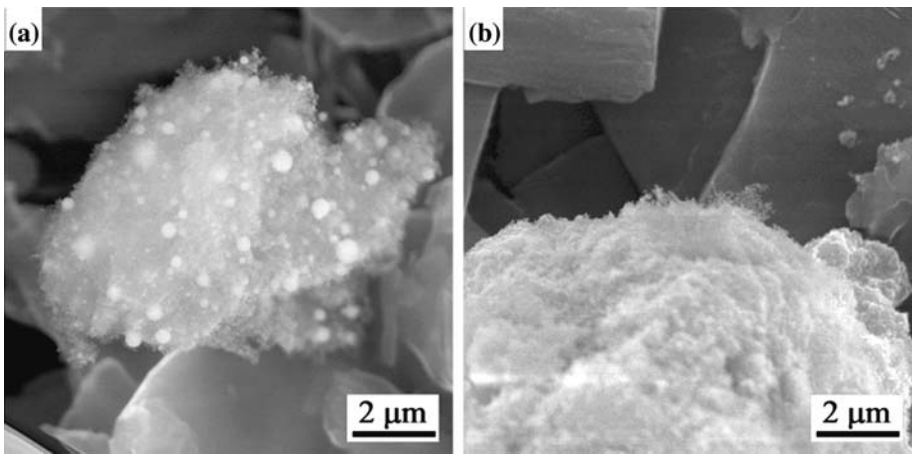

Figure 4. SEM images of FSP Yb/Si-mixed oxide ($X_{wt} = 0.5$) powder prepared from (a) ''Nitrile solution'' and (b) ''2-EHA solution''.

inhomogeneity and only consist of particles smaller than 10 nm as verified by TEM analysis (not shown here). Furthermore, the homogeneous Yb/Si-mixed oxide powder derived from the ''2-EHA solution'' is completely X-ray amorphous as illustrated in Figure 5 for powders with $X_{wt} = 0.2$ and 0.5 in contrast to the ''Nitrile solution''. The amorphous structure of the Yb/Si-mixed oxide for all ytterbium loadings investigated was further confirmed by a characteristic diffuse electron diffraction pattern (not shown).

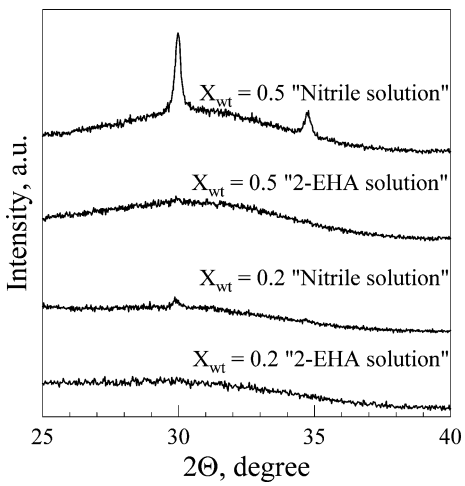

Figure 5. Comparison of X-ray diffraction patterns of powders derived from the ''Nitrile solution'' and the ''2-EAH solution'' for two different ytterbium oxide mass loadings ($X_{wt} = 0.5$ and 0.2). The diffraction signals at $2\Theta = 29.6°$ and 34.3° correspond to cubic ytterbium oxide planes [222] and [400], respectively (PDF: 43–1037).

Figure 6 reveals the homogeneous distribution of the ytterbium and silicon atoms of the powder synthesized with ''2-EHA solution''. The element specific images show the intense mixing of ytterbium and silicon within the primary particles. The mixing length between the Yb and Si atoms is much smaller than the primary particle scale. No individual ytterbium oxide or silicon oxide particles were observed. Similar distributions were also found for all other ytterbium loadings and Yb/Si-mixed oxides with distinctly different stoichiometry than the corresponding silicates.

Figure 7 shows the powder refractive index obtained with the Becke line method for the Yb/Si-mixed oxide powder as a function of the ytterbium oxide loading. The refractive index for pure silica and pure ytterbium oxide are 1.46 (Wypych, 1999) and 1.947 (Medenbach et al., 2001), respectively. Mixing the two oxides during the flame process increased the index of refraction linearly (Appen's law) with the molar loading of ytterbium above 0.01 ($X_{wt} > 0.03$). The refractive index is not affected by the powder homogeneity as revealed by comparison of the powders from ''2-EHA solution'' (circles) and ''Nitrile solution'' (squares). However, there is an abrupt increase of the measured refractive index from 1.44 to 1.49 when small amounts of ytterbium oxide ($X_{mol} = 0.01$) are added. The sharp refractive index increase for

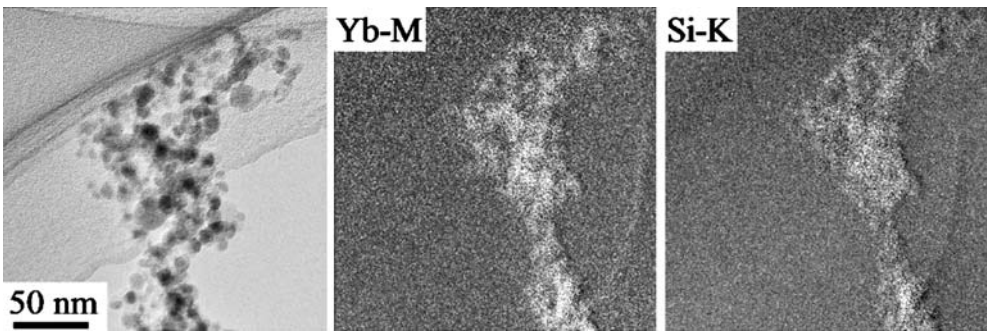

Figure 6. TEM micrograph (left) and Yb (middle) and Si (right) element specific images (ESI) of Yb/Si-mixed oxide ($X_{wt} = 0.5$) (“2-EHA solution”) powder.

small Yb_2O_3 contents coincided with the steep SSA increase shown in Figure 8.

Composite properties

Figure 9 shows the transparency of the Yb/Si-mixed oxide composite (16.5 wt% filler load). The filler powder was produced from “2-EHA solution” having an Yb_2O_3 content from $X_{wt} = 0$ to 0.5 (circles). The transparency decreases for increasing ytterbium content and plateaus at a transparency of 45% until the refractive index of the polymer (1.53) is matched at $X_{wt} = 0.3$ (see Figure 7) where the transparency decreases strongly upon addition of more ytterbium. Figure 9 also shows the composite transparency for Yb/Si-mixed oxide fillers produced from the “Nitrile solution” (squares). The composite transparency from the inhomogeneous powder (“Nitrile solution”) is drastically reduced (about five times) for Yb_2O_3 contents of $X_{wt} = 0.2$ and 0.5.

Table 1 summarizes the physical properties of three composites derived from three different fillers having a constant filler loading of 52 wt% (48 wt% polymer). The FSP derived Yb/Si-mixed oxide ($X_{wt} = 0.3$) filler was prepared with 8 ml/min liquid feed rate and 3 l/min dispersion gas resulting in a production rate of 19 g/h. The FSP material had a

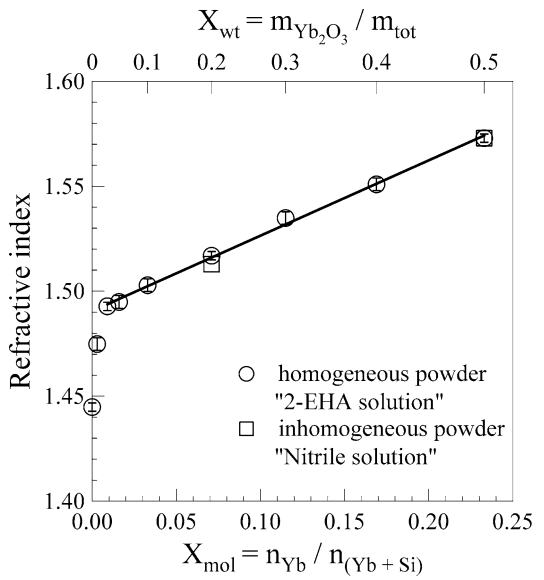

Figure 7. Refractive index of as prepared FSP Yb/Si-mixed oxide powder with $X_{wt} = 0$ to 0.5. The data is plotted against the mol fraction of ytterbium in accordance with Appen’s law (linear dependence).

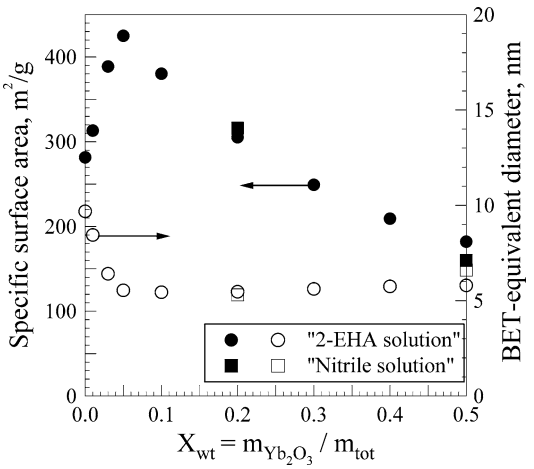

Figure 8. Specific surface area (SSA) and calculated BET-equivalent primary particle diameter (d_{BET}) of as prepared of FSP Yb/Si-mixed oxide powders having $X_{wt} = 0$ to 0.5.

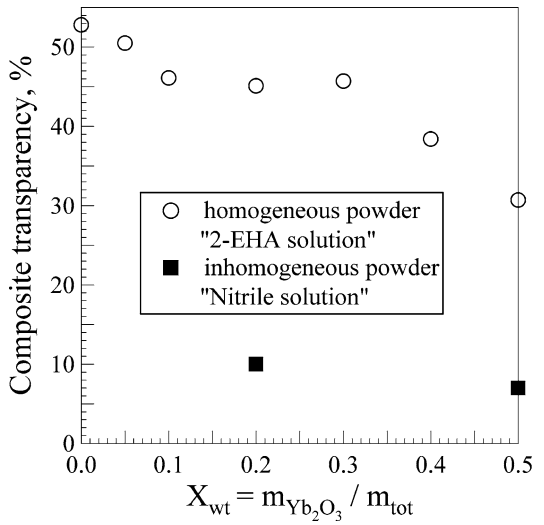

Figure 9. Transparency of the Yb/Si-mixed oxide composite (16.5 wt% filler load, filler derived from "2-EHA solution"). The filler had an Yb_2O_3 content of $X_{wt} = 0$ to 0.5.

SSA of 115 m^2/g and very similar flexural strength and E-modulus compared to a commercial SiO_2 filler (OX-50) and a mechanical mixture of SiO_2 (OX-50) and YbF_3. The disc-consistency and therefore the paste flowablity are only slightly lower than that of materials based on commercial fillers. Most notably, the FSP material yields the highest composite transparency compared to the commercial composites materials (30% increase compared to OX-50) and the highest radiopacity (20% increase compared to OX-50/YbF_3).

Discussion

Control of flame-made particles

The inhomogeneity of the powder prepared from the "Nitrile solution" is attributed to the low combustion enthalpy density of 5.6 kJ/g_{gas}. This value is slightly higher than the critical value of 4.7 kJ/g_{gas} in these systems (Jossen et al., In press) but the decomposition temperature of the nitrate complex (decomposition starts above 100°C in 2-ethylhexanoic acid and starts above 100°C in air (thermo-gravimetric measurement)) is significantly higher than the boiling point of the main solvent acetonitrile (82°C). This is in agreement with the general analysis of FSP criteria for powder homogeneity (Jossen et al., In press). In contrast the "2-EHA solution" has a combustion enthalpy density of 8.1 kJ/g_{gas} which is substantially higher than the critical value of 4.7 kJ/g_{gas} (Jossen et al., In press) leading to homogeneous particle formation.

The amorphous structure of the homogeneous Yb/Si-mixed oxide (Figure 5) is in agreement with former studies of zinc oxide doping of silica. For Zn molar concentrations below 0.4, the powder was amorphous and no reflections of ZnO appear in the XRD patterns (Tani et al., 2002). The maximum molar concentration of ytterbium investigated in this study was 0.233 ($X_{wt} = 0.5$). The strong interaction of the two metal species (Yb and Si) during oxide formation and subsequent particle growth is evident, particularly in contrast to the XRD patterns of two non-interacting species such as gold-doped silica made in a spray flame (Mädler et al., 2003) where it was shown that the formation mechanisms of the gold and the silica are independent from each other resulting in the formation of clearly XRD detectable gold clusters even at low loadings (1 wt%).

Yamamoto et al. (1999b) reported also an amorphous structure when preparing Yb/Si-mixed oxide (up to $X_{wt} = 0.62$) using wet chemical methods where an SiO_2 gel was impregnated with an aqueous solution of ytterbium nitrate. No distinct peaks in the XRD pattern were observed when pretreating at 1073 K for 1 h, indicating the

Table 1. Composite physical properties using Yb/Si-mixed oxide ($X_{wt} = 0.3$) filler (52 wt% filler, 48 wt% polymer) in comparison with commercial SiO_2 filling materials

	Flexural strength (MPa)	E-modulus (MPa)	Disc-consistency (mm)	Transparency (%)	Radiopacity (%) to Al standard
FSP Yb/Si-mixed oxide ($X_{wt} = 0.3$)	79 ± 8	4620 ± 180	21.1	13.2	180
OX-50	91 ± 9	5200 ± 160	23.8	10.1	20
YbF_3/OX-50	105 ± 5	4370 ± 110	27.4	9.5	150

ytterbium oxide did not crystallize. In contrast, clear ytterbium oxide diffractions signals are observed for the FSP-derived powder synthesized from the ''Nitrile solution'' (Figure 5). The diffraction signals at $2\Theta = 29.6°$ and 34.3° correspond to cubic ytterbium oxide planes [222] and [400] (PDF: 43-1037) corroborating the fact that pure ytterbium oxide crystallites are formed because of inhomogeneous precursor release (droplet residues) (Mädler & Pratsinis, 2002).

The high degree of mixing of the Si and Yb species during the powder synthesis in the flame is also evident from the specific surface area with regard to ytterbium loading (Figure 8). When small amounts of ytterbium are added ($X_{wt} < 0.05$) the specific surface area sharply increased from 280 m^2/g to 425 m^2/g regardless of the higher density material added leading to a sharp decrease in the BET-equivalent primary particle diameter from 9.6 to 5.9 nm. For $X_{wt} = 0.05$, the specific surface area started to decrease while the BET-equivalent primary particle diameter remained nearly constant. Similar behavior was observed in the zinc oxide/silica mixed system produced by the FSP process (Tani et al., 2002) where a remarkable decrease of the d_{BET} by a factor of 3.7 was observed when adding 20 mol% Zn to the silica precursor. This shows that small amounts of certain dopant atoms drastically influence particle formation. Tani et al. (2002) proposed a particle formation mechanism of the Zn/Si-mixed oxide systems in the flame process transferring bulk phase transition temperatures of the corresponding oxides to nanoparticle properties in the flame environment. The high dispersion of ZnO within the primary particle length scale was attributed to the fact that SiO_2 clusters preferentially form early in the flame because of the high boiling point of silica while the ZnO sublimation temperature is higher than the silica melting point. Therefore, ZnO can easily diffuse into the liquid silica before rapid cooling in the flame quenches this process. The Yb/Si-mixed oxide has similar properties regarding the fact that for ytterbium oxide the sublimation point is 2430°C which lies in the temperature region of boiling (2950°C) and melting (1713°C) of SiO_2 (Dean, 1999). Temperatures in the flame spray process are sufficiently high to support this formation mechanism (Mädler et al., 2002a) while atom specific images corroborate the atomic dispersion (Figure 6). This mechanism will primarily affect the surface of the silica particles were small amounts of ytterbium will quench the particle growth consistent with the observed sharp increase of the specific surface area and the refractive index for small ytterbium loadings (Figure 7). After saturation of ytterbium oxide within the particle, the refractive index follows the well known linear progression with the atomic content of the high refractive index material (Yb_2O_3).

Composite performance

The composite transparency of the homogeneous powder decreases slightly for increasing ytterbium oxide content possibly because of small powder inhomogeneities of the mixed oxide powder compared to the pure silica powder. However, within the region ($X_{wt} = 0.2$ to 0.3) where the refractive index of the polymer (1.53) is matched, the transparency remains constant with regard to the ytterbium loading. At that point the transmitted light does not interact with the particles/polymer interfaces since the particle composition is very homogeneous as corroborated by the high dispersion of Yb and Si in the particles (Figure 6) and amorphous mixed-oxide structure (Figure 5b and d). Incorporation of more ytterbium has a clear detrimental effect because the refractive index of the filler becomes significantly larger than that of the polymer. However, there is a significant loss in transparency (factor of five) for composites prepared from inhomogeneous powder (''Nitrile solution'', squares in Figure 9). This effect cannot be attributed to the overall elemental composition, refractive index (Figure 7) or to the overall specific surface area (Figure 8) of the filler as compared to the fillers prepared from the ''2-EHA solution''. The major difference of these filler materials is the presence of larger (about 100 nm) particles of pure crystalline ytterbium oxide. These particles possess a refractive index of 1.947 (Wypych, 1999) and will once embedded into the polymer matrix strongly interact with the transmitted light leading to diffraction and scattering events and a decrease in transparency. This phenomenon clearly demonstrates the importance of fundamentally understanding of particle formation in the flame controlling morphology and particle homogeneity (Mädler & Pratsinis, 2002; Mädler et al., 2002b; Jossen et al., In press).

The composite flexural strength and E-modulus of elasticity are similar to standard materials (Table 1). However, the reported high transparency and the high radiopacity make those composites made from FSP-fillers a superior material in biomedical applications and especially attractive for dental restoration.

Conclusion

Powder homogeneity plays a crucial role in optical applications of nanoparticles. This is demonstrated for flame-made mixed oxide nanoparticles applied as filling materials in transparent and radiopaque composites. Radiopacity is an important property of biomedical composites since it enables their detection/localization in X-ray scanning. High radiopaque composite materials have been obtained by co-precipitation of ytterbium oxide with the well established silica filler in the one step (FSP) flame process. The manufactured composite containing the FSP-filling material showed similar mechanical properties but a higher transparency than conventional fillers because of the achieved high atomic mixing of the two elements within the nanoparticles giving very homogeneous optical properties (refractive index). The importance of homogeneous mixing was further demonstrated by comparing homogeneous fillers with fillers having partly segregated particles of pure metal oxide. Despite the fact that this filler posed similar overall refractive index, specific surface area and elemental composition a drastically reduced transparency was observed.

Acknowledgment

The research was supported by the Kommission für Technologie und Innovation (KTI) TOP NANO 21, Grant No. 5929.1, Switzerland. We gratefully acknowledge the technical support on the refractive index measurements of H. Schulz and D. Stratakis (ETH Zurich). Stimulating discussions with Prof. S.E. Pratsinis, H. Schulz, R. Mueller, M.J. Height (ETH Zurich) are also gratefully acknowledged.

References

Asefa T., C. Yoshina-Ishii, M.J. MacLachlan & G.A. Ozin, 2000. New nanocomposites: Putting organic function "inside" the channel walls of periodic mesoporous silica, J. Mater. Chem. 10(8), 1751–1755.

Boury B. & R.J.P. Corriu, 2000. Adjusting the porosity of a silica-based hybrid material, Adv. Mater. 12(13), 989–992.

Choudhury K.R., J.G. Winiarz, M. Samoc & P.N. Prasad, 2003. Charge carrier mobility in an organic–inorganic hybrid nanocomposite, Appl. Phys. Lett. 82(3), 406–408.

Combe E.C., F.J.T. Burke & W.H. Douglas,. 1999. Dental Biomaterials. Boston: Kluwer Academic Publ.

Dean J.A., 1999. Table 3.2 Physical constants of inorganic compounds. Lange's Handbook of Chemistry, McGraw-Hill Inc., New York.

Guo S.Q., N. Hirosaki, Y. Yamamoto, T. Nishimura & M. Mitomo, 2001. Dependence of fracture stress on applied stress rate in a Yb_2O_3–SiO_2-doped hot-pressed silicon nitride ceramic, J. Mater. Res. 16(11), 3254–3261.

Hehlen M.P., N.J. Cockroft, T.R. Gosnell & A.J. Bruce, 1997. Spectroscopic properties of Er^{3+}- and Yb^{3+}-doped soda-lime silicate and aluminosilicate glasses, Phys. Rev. B 56(15), 9302–9318.

Jossen R., S.E. Pratsinis, W.J. Stark & L. Mädler. Criteria for flame-spray synthesis of hollow, shell-like or inhomogeneous oxides. J. Am. Ceram. Soc., In press.

Klapdohr S. & N. Moszner, 2005. Inorganic Components for dental filling composites. Monatsh. Chem. 136, 21–45.

Klemm H. & G. Pezzotti, 1994. Fracture-toughness and time-dependent strength behavior of low-doped silicon nitrides for applications at 1400°C, J. Am. Cer. Soc. 77(2), 553–561.

Krumeich F., H.J. Muhr, M. Niederberger, F. Bieri & R. Nesper, 2000. The cross-sectional structure of vanadium oxide nanotubes studied by transmission electron microscopy and electron spectroscopic imaging, Zeitschrift Fur Anorganische Und Allgemeine Chemie 626(10), 2208–2216.

Liang J.J., A. Navrotsky, T. Ludwig, H.J. Seifert & F. Aldinger, 1999. Enthalpy of formation of rare-earth silicates Y_2SiO_5 and Yb_2SiO_5 and N-containing silicate $Y_{10}(SiO_4)6N_2$, J. Mater. Res. 14(4), 1181–1185.

Mädler L., H.K. Kammler, R. Mueller & S.E. Pratsinis, 2002a. Controlled synthesis of nanostructured particles by flame spray pyrolysis, J. Aerosol Sci. 33(2), 369–389.

Mädler L. & S.E. Pratsinis, 2002. Bismuth oxide nanoparticles by flame spray pyrolysis, J. Am. Cer. Soc. 85(7), 1713–1718.

Mädler L., W.J. Stark & S.E. Pratsinis, 2002b. Flame-made ceria nanoparticles, J. Mater. Res. 17(6), 1356–1362.

Mädler L., W.J. Stark & S.E. Pratsinis, 2003. Simultaneous deposition of Au nanoparticles during flame synthesis of TiO_2 and SiO_2, J. Mater. Res. 18(1), 115–120.

McLean J.H., 1965. Significance of Becke Line refractive indices in synthetic fibers, Text. Res. J. 35(3), 242–244.

Medenbach O., D. Dettmar, R.D. Shannon, R.X. Fischer & W.M. Yen, 2001. Refractive index and optical dispersion of rare earth oxides using a small-prism technique, J. Opt. a-Pure Appl. Opt. 3(3), 174–177.

Morse T.F., 2003. US Patent 6 546 757 B1.

Moszner N. & S. Klapdohr, 2004. Nanotechnology for dental composites, Int. J. Nanotechnol. 1(1/2), 130–156.

Moszner N. & U. Salz, 2001. New developments of polymeric dental composites, Prog. Polym. Sci. 26(4), 535–576.

Mueller R., H.K. Kammler, S.E. Pratsinis, A. Vital, G. Beaucage & P. Burtscher, 2004. Non-agglomerated dry silica nanoparticles, Powder Technol. 140(1-2), 40–48.

Nussbaumer R.J., W. Caseri, T. Tervoort & P. Smith, 2002. Synthesis and characterization of surface-modified rutile nanoparticles and transparent polymer composites thereof, J. Nanoparticle Res. 4(4), 319–323.

Rheinberger V., U. Salz, W. Hoeland, A. Rumphorst, K. Grabher, U.K. Fischer, M. Schweiger & N. Moszner, 1999. Polymerizable dental composite material. Eur. Pat. Appl. EP 923925 A2 19990623, Liechtenstein.

Saveyn H., D. Mermuys, O. Thas & P. van der Meeren, 2002. Determination of the refractive index of water-dispersible granules for use in laser diffraction experiments, Part. Part. Syst. Char. 19(6), 426–432.

Schulz H., L. Mädler, S.E. Pratsinis, P. Burtscher & N. Moszner, 2005. Flame-made Ta_2O_5/SiO_2 particles with controlled refractive index and nanocomposite transparency. Adv. Funct. Mater. 15(5), 830–837.

Simpson J.O. & A.K. St. Clair, 1997. Fundamental insight on developing low dielectric constant polyimides. Thin Solid Films 308, 480–485.

Stoiber R.E. & S.A. Morse,. 1994. Crystal Identification with the Polarizing Microscope. London: Chapman & Hall.

Tani T., L. Mädler & S.E. Pratsinis, 2002. Synthesis of zinc oxide/silica composite nanoparticles by flame spray pyrolysis, J. Mater. Sci. 37(21), 4627–4632.

Toropov N.A. & I.A. Bondar, 1961. Silicates of the rare earth elements. Div. Chem. Sci. 8, 1278–1284.

Wu B., P.L. Chu & J. Arkwright, 1995. Ytterbium-doped silica slab waveguide with large nonlinearity, IEEE Photon. Technol. Lett. 7(12), 1450–1452.

Wypych G., 1999. Handbooks of Fillers. Toronto: Chem. Tec. Publishing.

Yamamoto T., T. Matsuyama, T. Tanaka, T. Funabiki & S. Yoshida, 1999a. Generation of acid sites on silica-supported rare earth oxide catalysts: Structural characterization and catalysis for alpha-pinene isomerization, Phys. Chem. Chem. Phys. 1(11), 2841–2849.

Yamamoto T., T. Tanaka, T. Matsuyama, T. Funabiki & S. Yoshida, 1999b. XAFS study of the structure of the silica-supported ytterbium oxide catalyst, Solid State Commun. 111(3), 137–142.

Zantner C., A.M. Kielbassa, P. Martus & K.H. Kunzelmann, 2004. Sliding wear of 19 commercially available composites and compomers, Dental Mater. 20(3), 277–285.